

Channel-Dependent Population Transfer: A Framework for Analyzing Complex Reaction Pathways

Amartya Bose^{1, a)} and Peter L. Walters^{2, 3, b)}

¹⁾*Department of Chemical Sciences, Tata Institute of Fundamental Research, Mumbai 400005, India*

²⁾*Department of Chemistry, University of California, Berkeley, California 94720, USA*

³⁾*Miller Institute for Basic Research in Science, University of California Berkeley, Berkeley, California 94720, USA^{c)}*

We present an approach of analyzing the transport of a quantum particle in a non-trivially connected extended system interacting with a dissipative medium. There are broadly two different aspects of the problem that affect the route taken by the transport process. First is obviously the couplings between the various sites, which translates into the intrinsic “strength” of a channel. Apart from the inter-site couplings, the solvents affecting the energies of the sites, and their relative coupling strengths and time-scales form the second factor. This impact of the such dissipative media is significantly more difficult to analyze. The Channel-Dependent Population Transfer (CDPT) method of analyzing the transport allows us to account for both the effects in a rigorous manner. We demonstrate the richness hidden behind the transport even for relatively simple systems — the effect of the local dissipative media is highly non-trivial and can mask the simplicity of the effect of the relative magnitude of the inter-site couplings. This opens up possibilities in terms of detailed study of the impact of factors on the nature of dynamics, especially possibilities of design of novel systems with an eye towards quantum control.

I. INTRODUCTION

Simulating complex chemical reactions in the condensed phase has been a holy grail of computational and theoretical chemistry. This already difficult task becomes even more arduous when the reaction involves the purely quantum mechanism of tunneling. However, this is ubiquitous in various processes like exciton transport in photosynthetic complexes, electron transfer, etc. In addition, many exciton and electron transfer processes happen in extended systems where there can be multiple pathways for the quantum “particle” to follow. A thorough understanding of the contribution of these various pathways is necessary to facilitate a more clear picture of the dynamics.

The simulation of the basic dynamics of quantum particles in a condensed phase is quite challenging in and of itself. Approximations like Redfield and Förster, though often used, are not universally applicable, especially in the strongly coupled regime. For numerically exact simulations of dynamics of extended systems, approaches based on tensor-networks have been gaining a lot of popularity. Most notable among them are density matrix renormalization group (DMRG)^{1–3} and its time-dependent variant.⁴ The family of multiconfiguration time-dependent Hartree (MCTDH)^{5,6} can also be thought of as being based on tree tensor networks. However, the approaches often fail to account for the effects of (a possible continuum of) translational and vibrational

degrees of freedom contributed by the solvent.

Methods based on simulating the reduced density matrix provide a lucrative alternative to the above-mentioned methods for simulating these systems. Of these, the quasi-adiabatic propagator path integral (QuAPI)⁷ and hierarchical equations of motion⁸ are the most widely used. Recently tensor networks have been shown to be exceptionally useful in increasing the efficiency of QuAPI.^{9–12} These ideas have also been successfully extended to a multisite framework capable of simulating the quantum dynamics of extended systems coupled with local dissipative media.^{13–15}

Despite the power and novelty of the methods discussed till now, they are unable to provide a clear and unambiguous insight into the mechanism of the transport. Consider an extended system with a non-trivial topology allowing for long-ranged couplings between sites, and assume we are interested in the transport of an exciton. For a given initial location of the exciton, the state-of-the-art simulations would yield the time-dependent population of the exciton on each of the sites. We would have no further information on the route or “pathway” that the exciton took to get to a particular site. Such information, however, is crucial to optimization of materials for guided quantum transport. An extremely naïve approach to analyzing the pathways would be to track the route of the strongest couplings in the system Hamiltonian that leads from the “source” to the “sink.” Such an approach would obviously miss out on the effects of the dissipative media. A different approach has been recently used to understand these pathways under a Lindbladian model Hamiltonian by evaluating the transport of the base system vis-a-vis a system with a particular chromophore dropped.¹⁶ The idea is that dropping a chromophore that is a part of the primary pathways would lead to a large

^{a)}Electronic mail: amartya.bose@tifr.res.in

^{b)}Electronic mail: peter.l.walters@gmail.com

^{c)}Both authors contributed equally to this work.

decrease of transport efficiency.

This paper proposes a method of analysis that while being independent of the underlying method of simulation, enables us to obtain critical information about the “pathway” of the quantum transport in presence of solvents. This Channel-Dependent Population Transfer (CDPT) method takes as a starting point the non-equilibrium rate¹⁷ generalization of the flux-based rate theory.^{18–20} Because the non-equilibrium rate theory captures the initial condition dependent transients, CDPT is capable of providing a time-dependent picture of how the transport happens across the various channels or pathways.

The paper is organized as follows. The method of analysis is outlined in Sec. II. Thereafter, CDPT is used to explore the dynamics in a coarse-grained four-site model of the Fenna-Matthews-Olson complex (FMO) with a focus on how this information can be used in a directed manner to gain detailed insights into the same. Finally, some concluding remarks and future outlook are presented in Sec. IV.

II. METHOD

Consider a system with N sites coupled with arbitrary harmonic baths. These baths may or may not be site-local. The Hamiltonian of such a problem is generally of the form:

$$\hat{H} = \hat{H}_0 + \hat{H}_{\text{SB}} \quad (1)$$

where \hat{H}_0 is the Hamiltonian corresponding to the system and \hat{H}_{SB} is the Hamiltonian corresponding to the system-bath coupling. (It is assumed that the system is represented in a basis that diagonalizes \hat{H}_{SB} .) Under Gaussian response, the harmonic baths are often obtained from a simulation of the bath response function.^{21,22} We define the *direct* population transfer from site k to site j or along the “channel” joining site k to site j as the population transfer between them without any intermediate site, also denoted by $P_{j\leftarrow k}$. The objective is to be able to simulate $P_{j\leftarrow k}$ as a function of time.

Though rate theory has historically been formulated in terms of equilibrium correlation functions,^{18,19} one of us has recently shown that it is possible to cast rate theory in a non-equilibrium framework that captures the initial condition-dependent transients.¹⁷ This non-equilibrium framework can be thought of as a direct calculation of the time derivative of the population of a particular site:

$$\frac{dP_j}{dt} = \text{Tr} \left[\tilde{\rho}(t) \hat{F}_j \right], \quad (2)$$

$$\text{where } \hat{F}_j = \frac{i}{\hbar} \left[\hat{H}_0, |j\rangle\langle j| \right]. \quad (3)$$

The rate is obtained as a “plateau” value of the time-dependent non-equilibrium flux, Eq. 2 and 3. This has recently been successfully applied to investigations of multistate problems.²³ However, here we are not interested

in a rate perspective. We rather want to understand the full time dynamics with additional information about the channel-dependent contributions. Expanding Eq. 2, one gets:

$$\frac{dP_j}{dt} = \frac{i}{\hbar} \sum_k \langle j | \tilde{\rho}(t) | k \rangle \langle k | \hat{H}_0 | j \rangle - \langle j | \hat{H}_0 | k \rangle \langle k | \tilde{\rho}(t) | j \rangle. \quad (4)$$

Now, for any k , one can interpret the term that gives a positive value as the rate of flow from k into j and the term with a negative magnitude as the rate of flow from j to k .

Thus, one can define the time-dependent population flow between the j^{th} and k^{th} sites as

$$P_{j\leftarrow k}(t) = \frac{i}{\hbar} \int_0^t dt \left(\langle j | \tilde{\rho}(t) | k \rangle \langle k | \hat{H}_0 | j \rangle - \langle j | \hat{H}_0 | k \rangle \langle k | \tilde{\rho}(t) | j \rangle \right). \quad (5)$$

For a real symmetric time-independent system Hamiltonian,

$$P_{j\leftarrow k}(t) = -\frac{2}{\hbar} \langle j | \hat{H}_0 | k \rangle \int_0^t dt \text{Im} \langle j | \tilde{\rho}(t) | k \rangle. \quad (6)$$

This is the working equation of CDPT. The method is independent of how the simulation was done, and therefore can be applied to any level of simulation as desired. There are no further approximations over and above the ones used for simulating the time-dependent reduced density matrix of the system. Notice that Eqs. 5 and 6 uphold detailed balance in the sense that $P_{j\leftarrow k}(t) = -P_{k\leftarrow j}(t)$ and that $P_{j\leftarrow j}(t) = 0$ for all j , encoding the fact that there cannot be any population transfer from a site to itself. It is also noteworthy that the imaginary part of the coherence encodes the corresponding channel-dependent population transfer.

Finally, the time dependent population of the j^{th} site can be expressed as

$$P_j(t) = P_j(0) + \sum_{k \neq j} P_{j\leftarrow k}(t). \quad (7)$$

Therefore, because the simulations are done starting from the relevant non-equilibrium initial condition, no information is lost in this CDPT analysis. If the system is thought of as a graph, with the sites being the vertices and the edges being the various inter-site connections, then the CDPT decomposes the time-evolution of the population on a site (vertex) along all the edges that are incident on it.

III. RESULTS

To demonstrate the utility of CDPT, we use it to explore how changes in the solvent affect the flow of an exciton through a system. The system used here is based

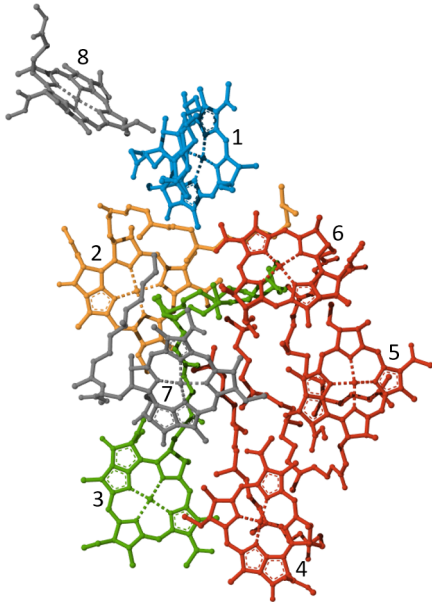
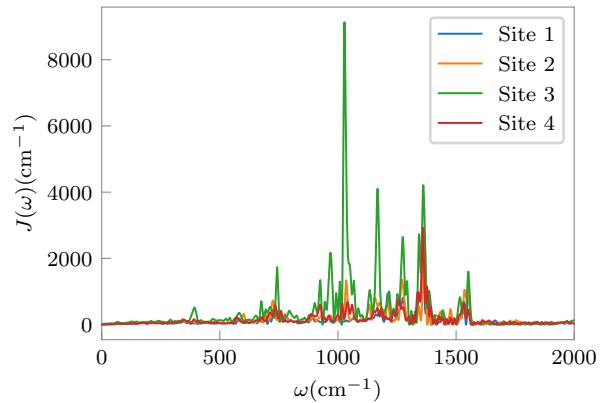


FIG. 1. Fenna-Matthews-Olson complex with the bacteriochlorophyll units colored by the coarse-grained units used. Blue: Coarse-grained site 1. Orange: Coarse-grained site 2. Green: Coarse-grained site 3. Red: Coarse-grained site 4. Gray: Ignored.

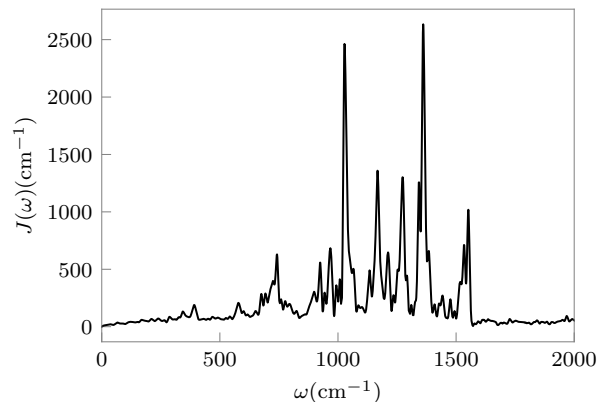
on the FMO complex. FMO is a naturally occurring light-harvesting complex with eight bacteriochlorophyll monomeric sites. It is ubiquitous as a model for excitonic transport and provides a very rich set of dynamical features owing to the non-linear inter-site couplings. We will illustrate the capabilities of the CDPT analysis through a systematic unraveling of the complexity in the excitonic dynamics. To enable a thorough exploration of the impact of the vibrational modes on the transfers through various channels, we simplify the system by coarse-graining it to include the four most relevant sites. For FMO, it is known that if bacteriochlorophyll site 1 is initially excited, the primary pathway is $1 \rightarrow 2 \rightarrow 3$ and the secondary pathway leads from $1 \rightarrow 6 \rightarrow 5 \rightarrow 4 \rightarrow 3$. Thus, in our coarse grained model we keep sites 1, 2, and 3 as is, reduce sites 4, 5, and 6 into a new renormalized 4th site and omit sites 7 and 8 entirely. This is shown in Fig. 1. Similar to the full FMO, we expect the model to have a primary pathway of $1 \rightarrow 2 \rightarrow 3$ and a secondary pathway of $1 \rightarrow 4 \rightarrow 3$.

The coarse-grained FMO model along with its interactions with the local vibrational baths is described by the following Hamiltonian:

$$\hat{H} = \hat{H}_0 + \hat{H}_{\text{SB}}, \quad (8)$$



(a) Site-dependent spectral densities



(b) Average spectral density

FIG. 2. Site-dependent and average spectral densities for the first four bacteriochlorophyll units in FMO obtained from Ref.²⁴.

$$\begin{aligned} \hat{H}_0 &= \sum_{k=1}^4 \epsilon_k |k\rangle\langle k| + \sum_{j \neq k} h_{j,k} |j\rangle\langle k|, \quad (9) \\ \hat{H}_{\text{SB}} &= \sum_{k=1}^4 \sum_{j=1}^{N_{\text{osc}}} \frac{p_{kj}^2}{2m_{kj}} + \frac{1}{2} m_{kj} \omega_{kj}^2 \left(x_{kj} - \frac{c_{kj} |k\rangle\langle k|}{m_{kj} \omega_{kj}^2} \right)^2, \quad (10) \end{aligned}$$

where ω_{kj} and c_{kj} are the frequency and coupling of the j^{th} harmonic mode of the bath corresponding to the k^{th} site. The electronic excitation energies are given by ϵ_k and the inter-site couplings are given by $h_{j,k}$.

The frequencies and couplings of the baths are characterized by the spectral density defined as

$$J_k(\omega) = \frac{\pi}{2} \sum_j \frac{c_{kj}^2}{m_{kj} \omega_{kj}} \delta(\omega_{kj} - \omega). \quad (11)$$

This can be calculated as the Fourier transform of the energy-gap autocorrelation function simulated using molecular dynamics. The site-dependent spectral densities and Hamiltonian for FMO have been recently simu-

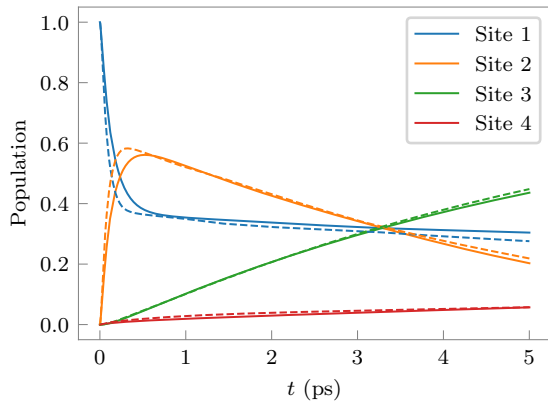


FIG. 3. Excitonic population on different sites as a function of time. Solid line: Average spectral density. Dashed line: Different spectral densities.

lated using the TD-LC-DFTB density functional.²⁴ We use these parameters as the starting point for our exploration. The Hamiltonian corresponding to this coarse-grained model is given in the supplementary information. The average and the site-dependent spectral densities are shown in Fig. 2 for reference.

Figure 3 shows the excitonic population corresponding to each of the sites for the site-specific and average spectral densities. (This information can, in principle, be calculated using many methods. Here the simulations have been conducted using the tensor network path integral method¹¹ based on Feynman-Vernon influence functional.) We notice that changing the average spectral density to the site-specific spectral densities has minor effects on the dynamics of bacteriochlorophyll sites 1 and 2 and negligible effects on the populations of sites 3 and 4. A key drawback of this population picture is that it washes away a lot of details. At this level, one cannot answer questions such as how does the transfer from site 1 to site 2, $P_{2\leftarrow 1}(t)$, change in switching between the two descriptions. Or what happens to the various contributions to the site 3 population?

The CDPT analysis presented in this paper allows us to answer these questions. In Fig. 4, we show the population dynamics of specific sites along with the individual contributions. The first thing that one immediately observes is that the primary flow of excitonic population happens along $1 \rightarrow 2 \rightarrow 3$. A secondary, slower, pathway that leads from site 1 to site 3 via site 4 ($1 \rightarrow 4 \rightarrow 3$) is also clearly visible. Additionally, one sees a non-insignificant contribution from $1 \rightarrow 2 \rightarrow 4 \rightarrow 3$. The direct transfer from site 1 to site 3 is the least important of these. While the ability to analyze the primary pathways immediately is obvious from Fig. 4, we would like to emphasize the power of the method in terms of disqualifying unimportant pathways as well. Notice that though site 1 transfers population into site 4, site 4 only transfers population into site 3. Therefore, a path like $1 \rightarrow 4 \rightarrow 2 \rightarrow 3$ is not

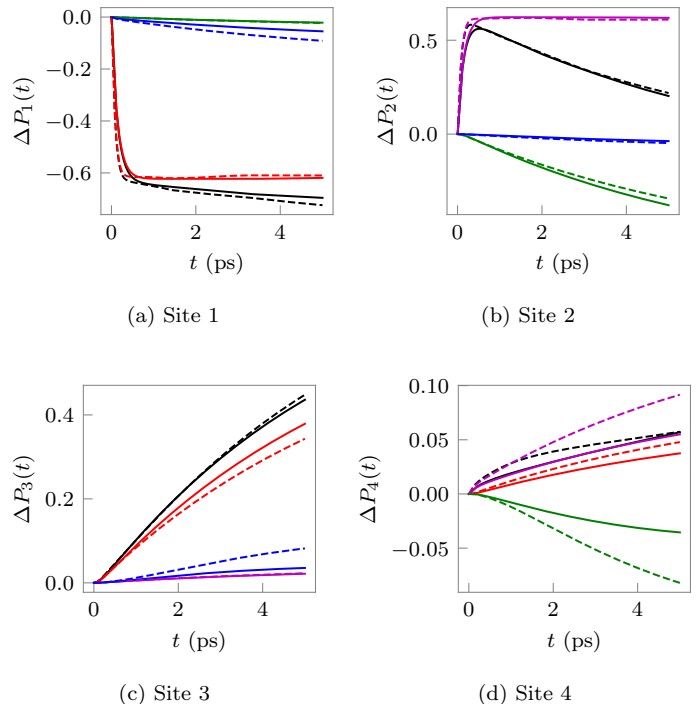


FIG. 4. Transfer pathways of excitonic population corresponding to each site with different spectral densities. Solid line: average bath. Dashed line: Different spectral densities. Black: Total change of population of the site. Magenta: Change due to site 1 ($P_{*←1}(t)$). Red: Change due to site 2 ($P_{*←2}(t)$). Green: Change due to site 3 ($P_{*←3}(t)$). Blue: Change due to site 4 ($P_{*←4}(t)$).

important.

Till now we were just discussing various important pathways. Looking at the excitonic population, Fig. 3, it is not clear what effect site-specific spectral densities have on the dynamics. With a CDPT analysis (Fig. 4), however, things become much clearer. We see that with the site-specific spectral densities the excitonic flow along $1 \rightarrow 2 \rightarrow 3$ is decreased coupled with an increased flow along the $1 \rightarrow 4 \rightarrow 3$ pathway. As for the other two pathways, the flow along $1 \rightarrow 2 \rightarrow 4 \rightarrow 3$ increases, and the direct transfer $1 \rightarrow 3$ remains the same. These changes in the excitonic pathways are evidenced by the fact that in going from the average to the site specific spectral densities, the direct transfer from site 2 to site 3 (red curve in Fig. 4 (c)) shows a decrease and the transfer from 4 to 3 (blue curve in the same figure) shows an increase. Furthermore, while there is an increase in both the transfer from site 1 to site 4 (magenta curve in Fig. 4 (d)) and site 2 to site 4 (red curve in the same figure), the increase in $1 \rightarrow 4$ is much larger. An explanation for these changes can be made by looking at $P_{3\leftarrow 2}(t)$ (red curve in Fig. 4 (c)). We notice that for the site-specific spectral densities, the direct transfer from site 2 to 3 seems to be somewhat restricted causing a rerouting of the excitation through site 4.

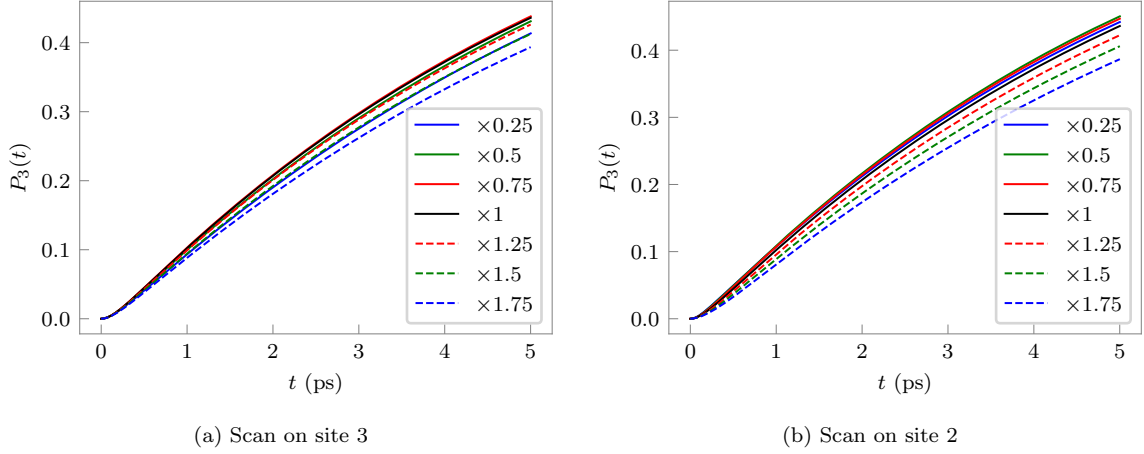


FIG. 5. Total population of site 3 as a function of time on scanning the reorganization energies on site 3 and site 2 respectively.

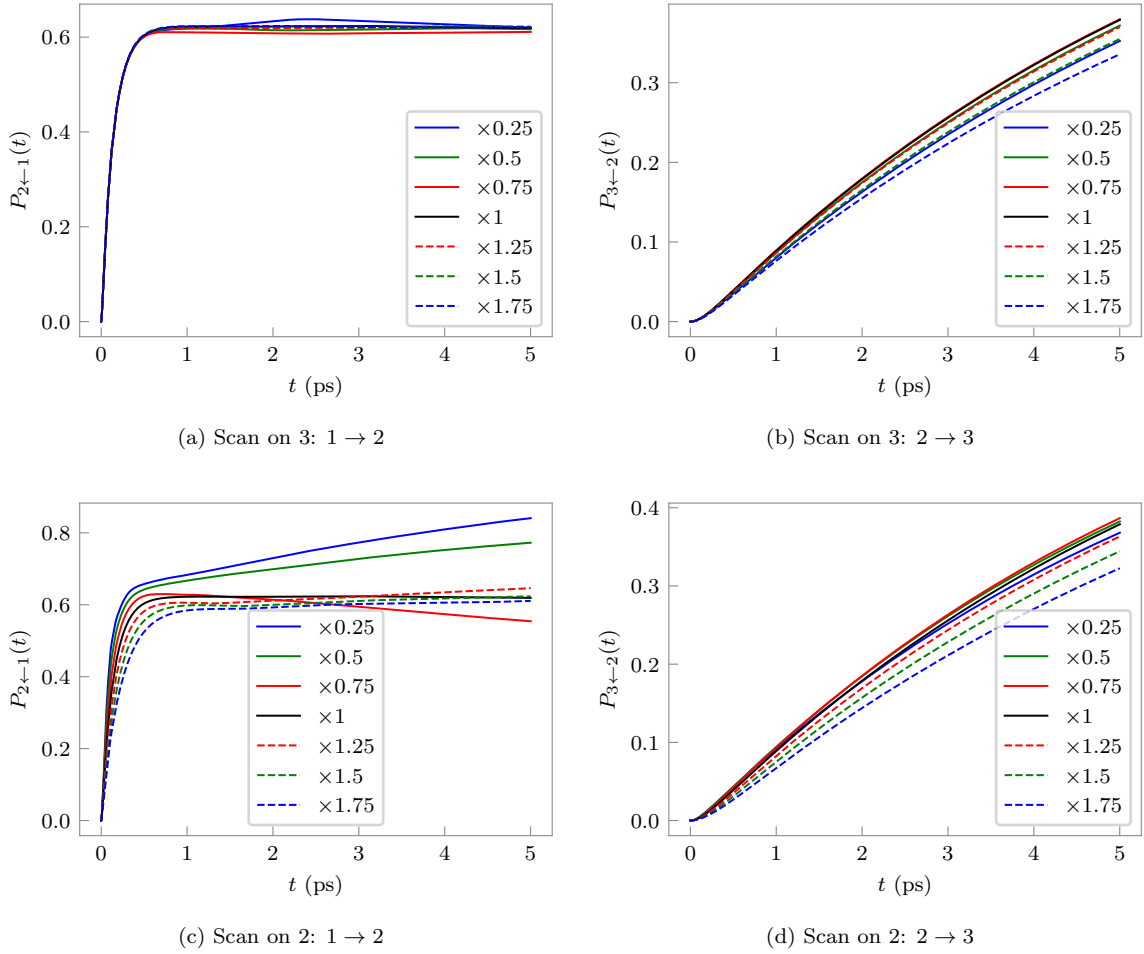


FIG. 6. Population transfer along $1 \rightarrow 2$ and $2 \rightarrow 3$ for components of the primary pathway when the site-specific reorganization energies on site 3 and site 2 are scanned.

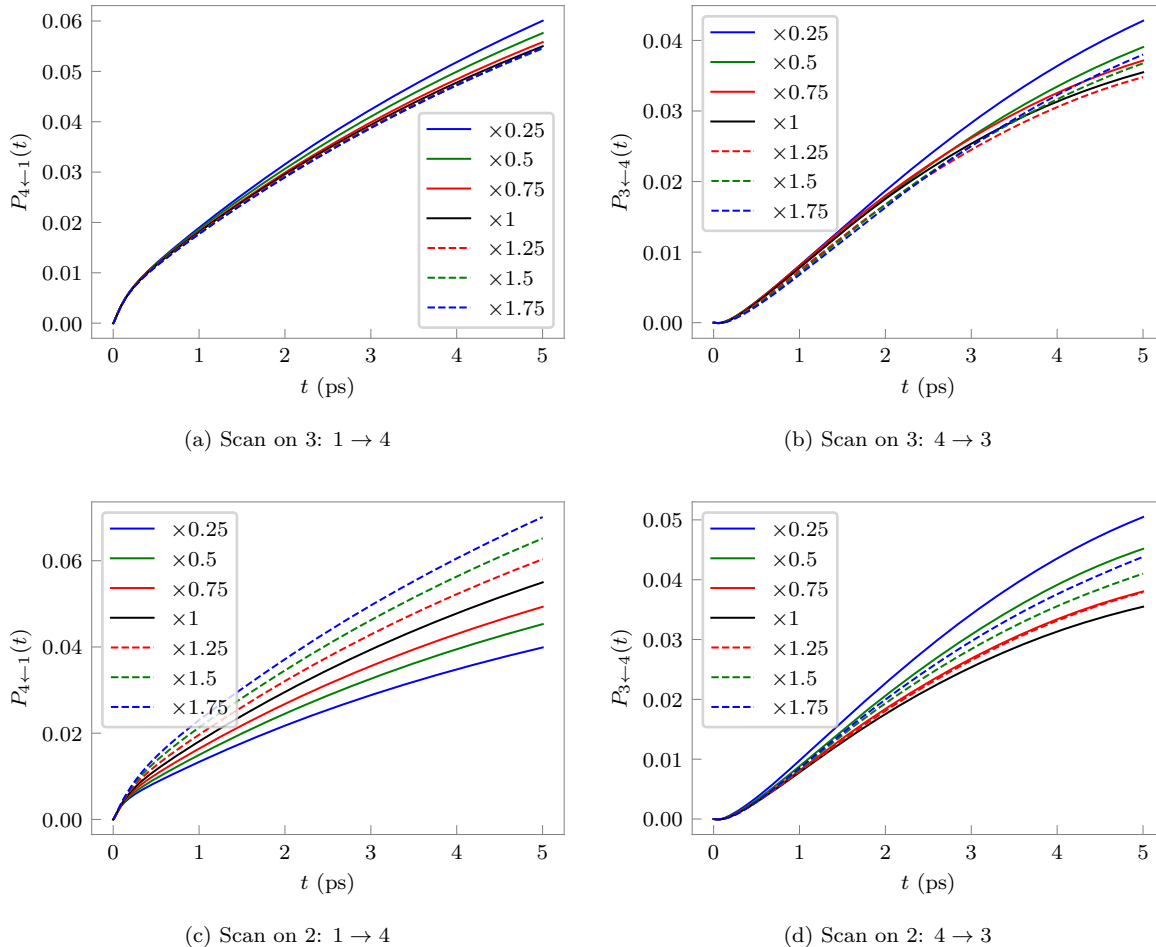


FIG. 7. Population transfer along $1 \rightarrow 4$ and $4 \rightarrow 3$ for components of the primary pathway when the site-specific reorganization energies on site 3 and site 2 are scanned.

Apart from this rather broad overview of the pathways of excitation dynamics, a CDPT analysis can uncover a wide variety of other features. For example, we can determine that the actual direct transfer from site 1 to site 2, $P_{2 \leftarrow 1}(t)$, stops after around 0.5 ps. Thus, the red line in Fig. 4 (a) and the magenta line in Fig. 4 (b) becomes practically flat around that time. This is the case even though the populations of both sites 1 and 2 keep changing throughout the period of simulation. Additionally, on careful observation of the plots Figs. 4 (a) and (b), it is seen that around 3 ps – 4 ps, there is a backflow of population from site 2 to site 1 in case of different baths. (Notice the small bump in the dashed red line in Fig. 4 (a) around that point.)

To explore the effect of the site-dependence of the spectral density, we systematically change the reorganization energies on single sites using the average bath as a starting point. We scale the reorganization energies on site 3 and site 2 with factors ranging from 0.25 and 1.75 in steps of 0.25. Figure 5 shows the change in the population dynamics of site 3. Notice that in both cases,

the population curve initially increases but then starts to decrease, though the reorganization energy where the maximum transfer occurs is different in the two cases. This behavior is similar to the inverted region in Marcus theory of electron transfer.²⁵ It is interesting that although the maximum transfer is obtained at different energies, at their respective maximum reorganization energies, the two curves look remarkably similar. However, this apparent similarity hides differences in the mechanism.

Let us consider the two pathways — the primary one, $1 \rightarrow 2 \rightarrow 3$ and the secondary one, $1 \rightarrow 4 \rightarrow 3$ separately. Figure 6 demonstrates the changes on the population dynamics along the primary pathway. In Fig. 6 (b) and (d), we see that the curves are very similar to Fig. 5 (a) and (b). This implies that the transfer $2 \rightarrow 3$ accounts for the main parts of the dynamics of the excitation population on site 3. Interestingly, the transfer from $1 \rightarrow 2$ seems to plateau and vary slightly around a constant value. However, things become completely different when the reorganization energy on site 2 is scanned (Figs. 6 (c) and (d)).

There is apparently very little pattern to the transfer from site 1 to site 2 as seen in Fig. 6 (c). The lack of a Marcus-like inversion region is because of the relatively large coupling between sites 1 and 2 which breaks perturbation theory. Additionally, in all these simulations, one finds that the transfer from site 1 to site 2 happens at the smallest time-scales. The transfer from site 2 to site 3, in Fig. 6 (b) and (d), seems to hit a maximum and decrease as we go away from it. This behavior is similar to the inverted region of Marcus theory of rate of electron transfer.

Finally, let us turn our attention to the secondary pathway of $1 \rightarrow 4 \rightarrow 3$. The impact of the scans on the two direct transfers that make up this pathway are shown in Fig. 7. First notice that on scanning the reorganization energy on site 3 (Fig. 7 (a) and (b)), both the direct transfers seem to decrease with the reorganization energy and then stop changing. When scanning the reorganization energy on site 2, the transfer from $1 \rightarrow 4$ seems to increase monotonically. However, the transfer from $4 \rightarrow 3$ shows a decrease followed by an increase, resulting in a minimum of amount of transfer. These changes caused in the $1 \rightarrow 4 \rightarrow 3$ pathway is very surprising, given that the reorganization energy on site 2, which is not a part of this pathway, is being scanned. (The data corresponding to the other channels, though not explored here, has been shown in the supplementary information for completeness.)

IV. CONCLUSION

Many exact and approximate methods exist that can simulate dynamics in complex systems coupled with solvents and vibrational modes. However, it is a significantly different and more difficult challenge to understand the exact routes that the transport process takes. Naïve approaches of looking at the inter-site couplings fall short because of their failure to account for the non-trivial effects of the solvent modes. In this paper, we have presented a novel technique for analyzing the dynamics that yields the contribution of each channel.

The channel dependent population transfer (CDPT) analysis is conducted on the time-evolved reduced density matrix. It is independent of the method of simulation of the dynamics and the approximations involved. While decomposing the population dynamics in terms of the contributions of various channels directly is not possible, an alternate route is found in terms of the time-derivatives. Starting from the non-equilibrium formulation of flux-based rate theory, we show that the individual terms in the equation can be thought of as rates of population transfer between a particular pair of sites. Integrating these equations, one can partition the full population dynamics as well. This is the core of CDPT.

Using this method of analysis, we can start to untangle the dynamics of systems with complex inter-site couplings. As demonstrated in the 4-site model based on

the FMO, the insights uncovered can often be very non-trivial. From a fundamental perspective, just because the total population on a site has a relatively regular pattern, it is not necessary that the regularity is there in all the individual contributions. Similarly, the total population showing some strange feature does not imply the existence of the weirdness in each of the contributory dynamics. What is possibly equally important to a fundamental understanding is the fact that changing the vibrational profile on a single site not only affects the pathways involving that site, but other pathways as well. This has important implications in trying to design materials and engineer specific outcomes in complex open quantum systems.

The analysis of channel-dependent population transfer reveals a wealth of information that lay hidden in the dynamics of the reduced density matrix. It is now possible to associate causes with various changes that happen in the total population dynamics. In the near future, we will demonstrate the utility of CDPT in understanding other processes beyond exciton transport, like proton-coupled electron transfer. CDPT promises to be an extremely important addition to our toolboxes for analyzing complex reactions and processes in the presence of thermal solvents. Finally, the fact that CDPT is not dependent on any single method of simulation of the time evolution of the reduced density matrix makes the analysis framework universally applicable.

- ¹S. R. White, “Density matrix formulation for quantum renormalization groups,” *Physical Review Letters* **69**, 2863–2866 (1992).
- ²U. Schollwöck, “The density-matrix renormalization group,” *Reviews of Modern Physics* **77**, 259–315 (2005).
- ³U. Schollwöck, “The density-matrix renormalization group: A short introduction,” *Philosophical Transactions of the Royal Society A: Mathematical, Physical and Engineering Sciences* **369**, 2643–2661 (2011).
- ⁴S. R. White and A. E. Feiguin, “Real-Time Evolution Using the Density Matrix Renormalization Group,” *Physical Review Letters* **93**, 076401 (2004).
- ⁵M. Beck, “The multiconfiguration time-dependent Hartree (MCTDH) method: A highly efficient algorithm for propagating wavepackets,” *Physics Reports* **324**, 1–105 (2000).
- ⁶H. Wang and M. Thoss, “Multilayer formulation of the multiconfiguration time-dependent Hartree theory,” *The Journal of Chemical Physics* **119**, 1289–1299 (2003).
- ⁷N. Makri and D. E. Makarov, “Tensor propagator for iterative quantum time evolution of reduced density matrices. I. Theory,” *The Journal of Chemical Physics* **102**, 4600–4610 (1995).
- ⁸Y. Tanimura and R. Kubo, “Time Evolution of a Quantum System in Contact with a Nearly Gaussian-Markoffian Noise Bath,” *Journal of the Physical Society of Japan* **58**, 101–114 (1989).
- ⁹A. Strathearn, P. Kirton, D. Kilda, J. Keeling, and B. W. Lovett, “Efficient non-Markovian quantum dynamics using time-evolving matrix product operators,” *Nature Communications* **9** (2018), 10.1038/s41467-018-05617-3.
- ¹⁰M. R. Jørgensen and F. A. Pollock, “Exploiting the Causal Tensor Network Structure of Quantum Processes to Efficiently Simulate Non-Markovian Path Integrals,” *Physical Review Letters* **123**, 240602 (2019).
- ¹¹A. Bose and P. L. Walters, “A tensor network representation of path integrals: Implementation and analysis,” *arXiv pre-print server* (2021), arxiv:2106.12523.
- ¹²A. Bose, “Pairwise connected tensor network representation of path integrals,” *Physical Review B* **105**, 024309 (2022).

- ¹³A. Bose and P. L. Walters, "A multisite decomposition of the tensor network path integrals," *The Journal of Chemical Physics* **156**, 024101 (2022).
- ¹⁴A. Bose and P. L. Walters, "Effect of temperature gradient on quantum transport," *Physical Chemistry Chemical Physics* **24**, 22431 (2022).
- ¹⁵A. Bose and P. L. Walters, "Tensor Network Path Integral Study of Dynamics in B850 LH2 Ring with Atomistically Derived Vibrations," *Journal of Chemical Theory and Computation* **18**, 4095–4108 (2022).
- ¹⁶L. A. Baker and S. Habershon, "Robustness, efficiency, and optimality in the Fenna-Matthews-Olson photosynthetic pigment-protein complex," *J. Chem. Phys.* **143**, 105101 (2015).
- ¹⁷A. Bose and N. Makri, "Non-equilibrium reactive flux: A unified framework for slow and fast reaction kinetics," *The Journal of Chemical Physics* **147**, 152723 (2017).
- ¹⁸W. H. Miller, "Quantum mechanical transition state theory and a new semiclassical model for reaction rate constants," *The Journal of Chemical Physics* **61**, 1823–1834 (1974).
- ¹⁹W. H. Miller, S. D. Schwartz, and J. W. Tromp, "Quantum mechanical rate constants for bimolecular reactions," *The Journal of Chemical Physics* **79**, 4889–4898 (1983).
- ²⁰A. Bose and N. Makri, "Quantum-classical path integral evaluation of reaction rates with a near-equilibrium flux formulation," *International Journal of Quantum Chemistry* **121** (2021), 10.1002/qua.26618.
- ²¹N. Makri, "The Linear Response Approximation and Its Lowest Order Corrections: An Influence Functional Approach," *The Journal of Physical Chemistry B* **103**, 2823–2829 (1999).
- ²²A. Bose, "Zero-cost corrections to influence functional coefficients from bath response functions," *The Journal of Chemical Physics* **157**, 054107 (2022).
- ²³R. Dani and N. Makri, "Quantum State-to-State Rates for Multistate Processes from Coherences," *J. Phys. Chem. Lett.* **13**, 8141–8149 (2022).
- ²⁴S. Maity, B. M. Bold, J. D. Prajapati, M. Sokolov, T. Kubař, M. Elstner, and U. Kleinekathöfer, "DFTB/MM Molecular Dynamics Simulations of the FMO Light-Harvesting Complex," *The Journal of Physical Chemistry Letters* **11**, 8660–8667 (2020).
- ²⁵R. A. Marcus, "Chemical and Electrochemical Electron-Transfer Theory," *Annu. Rev. Phys. Chem.* **15**, 155–196 (1964).